



RESEARCH LETTER

10.1002/2016GL069261

Key Points:

- Microfluidic setup provides a controlled way of observing the reactive-infiltration instability
- Experimentally measured instability wavelength compares favorably to the theoretical prediction
- This experimental setup can also be used to determine the intrinsic reaction rate of minerals

Correspondence to:

P. Szymczak,
Piotr.Szymczak@fuw.edu.pl

Citation:

Osselin, F., P. Kondratiuk, A. Budek, O. Cybulski, P. Garstecki, and P. Szymczak (2016), Microfluidic observation of the onset of reactive-infiltration instability in an analog fracture, *Geophys. Res. Lett.*, 43, 6907–6915, doi:10.1002/2016GL069261.

Received 21 APR 2016

Accepted 20 JUN 2016

Accepted article online 24 JUN 2016

Published online 12 JUL 2016

Microfluidic observation of the onset of reactive-infiltration instability in an analog fracture

F. Osselin¹, P. Kondratiuk¹, A. Budek², O. Cybulski³, P. Garstecki³, and P. Szymczak¹

¹Institute of Theoretical Physics, Faculty of Physics, University of Warsaw, Warsaw, Poland, ²Institute of Geophysics, Polish Academy of Sciences, Warsaw, Poland, ³Institute of Physical Chemistry, Polish Academy of Sciences, Warsaw, Poland

Abstract Reactive-infiltration instability plays an important role in many geophysical problems yet theoretical models have rarely been validated experimentally. We study the dissolution of an analog fracture in a simple microfluidic setup, with a gypsum block inserted in between two polycarbonate plates. By changing the flow rate and the distance between the plates, we are able to scan a relatively wide range of Péclet and Damköhler numbers, characterizing the relative magnitude of advection, diffusion, and reaction in the system. We quantify the characteristic initial wavelengths of the perturbed fronts during the onset of instability. The results agree well with theoretical predictions based on linear stability analysis, thus experimentally validating current reactive-infiltration instability theory and opening new opportunities for experimental assessment of mineral reactivity.

1. Introduction

Petroleum engineers were first to notice that the dissolution around the acidized well is often nonuniform and the flow becomes spontaneously localized in pronounced channels, which they have called “wormholes” [Rowan, 1959]. They have learned how to use them to their advantage—wormholes transport flow in an effective manner while not requiring a lot of reactant for their creation; hence, they provide an efficient way of increasing the permeability of the rock. It soon turned out that these instabilities are not only relevant to the acidized wellbores, but they can take place in almost any system in which the surface reaction is coupled with the fluid flow, hence the name *reactive-infiltration instability* coined by Chadam et al. [Chadam et al., 1986; Ortoleva et al., 1987; Steefel and Lasaga, 1990]. The instability is caused by a positive feedback between the reaction and fluid flow: a faster reaction locally leads to a permeability increase, which speeds up the local flow allowing the reactant to penetrate deeper inside the matrix. The range of length scales spanned by these phenomena is impressive—from the centimeter scale redox front fingering in siltstones [Ortoleva, 1994] and skarn [Ciobanu and Cook, 2004] to kilometer-long scalloping of a dolomitization front advancing into limestone [Merino, 2011] or of uranium rolls [Dahlkamp, 2009]. The associated range of timescales is also huge—whereas fast-reacting systems, like acidized limestone cores [Hoefner and Fogler, 1988] or plaster [Daccord, 1987; Daccord and Lenormand, 1987], or salt flushed with water in a Hele-Shaw cell [Kelemen et al., 1995; Golfier et al., 2002], show fingering on the scale of minutes, the geological structures evolve much more slowly, over hundreds of thousands of years. Moreover, the reactive-infiltration instability is not limited to the groundwater flowing through porous rocks, but as first shown by Aharonov et al. [1995] is also relevant to the magma flows, which also become focused in high-porosity channels, which can be observed in igneous rocks in forms of permeable dunite (olivine rock) conduits embedded in the less permeable matrix [Spiegelman et al., 2001]. The formation of dunite fingers during reaction between olivine-saturated liquid and harzburgite has also been experimentally demonstrated on a centimeter scale by Daines and Kohlstedt [1994] and Pec et al. [2015]. In recent years, the relevance of these problems to the CO₂ sequestration have increased the interest in the subject [Luquot and Gouze, 2009; Ellis et al., 2011; Elkhoury et al., 2013; Hao et al., 2013; Deng et al., 2013; Carroll et al., 2013; Smith et al., 2013; Elkhoury et al., 2015; Fu et al., 2015; Menke et al., 2015; García Ríos, 2015; Hidalgo et al., 2015]. Finally, reactive-infiltration instability is also a key factor in cave formation processes [Groves and Howard, 1994; Hanna and Rajaram, 1998; Szymczak and Ladd, 2011; Cabeza et al., 2015].

The theoretical basis of the reactive-infiltration instability is now relatively well understood, with the linear stability analysis carried out both for the dissolving porous medium [Chadam et al., 1986; Ortoleva et al., 1987; Sherwood, 1987; Hinch and Bhatt, 1990; Szymczak and Ladd, 2014] and for fractures [Szymczak and Ladd, 2012].

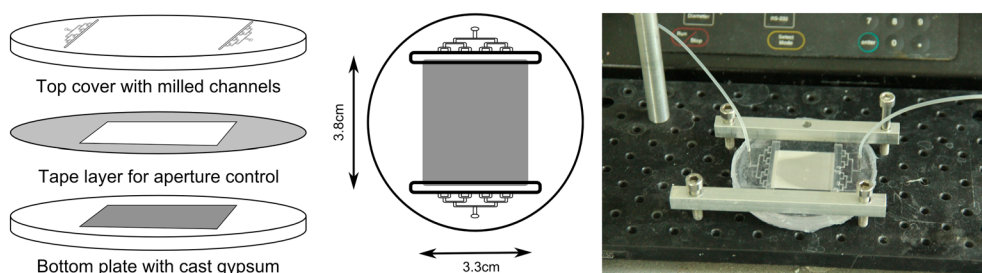


Figure 1. (left) The experimental setup. The chip is a sandwich of three layers. The top, polycarbonate plate has a network of microfluidic channels that deliver a uniform flow of the liquid into the inlet reservoirs and an outlet network of channels. The bottom plate is flat apart from a shallow rectangular indentation filled with gypsum. The surface of the plaster is perfectly flat and leveled with the surface of the plastic. A thin foil is inserted in between the two plastic layers to control the spacing. (right) A photograph of the experimental setup.

Still, the experimental studies invariably focus on the later stages of the dissolution process, dominated by the competition between the fully grown wormholes [Daccord, 1987; Hoefner and Fogler, 1988; Golfier et al., 2002; Detwiler et al., 2003; Polak et al., 2004; Luquot and Gouze, 2009; Noiriél et al., 2013; Luquot et al., 2014; Ott and Oedai, 2015]. In contrast, experimental observation of the onset of the instability has always been an issue because of a variety of reasons. First, the dissolving medium should be sufficiently uniform so that the presence of heterogeneities would not affect the initial flow distribution too much, thus preventing the observation of the spontaneous development of the instability [Kalia and Balakotaiah, 2009; Upadhyay et al., 2015]. Second, the experimental setup should allow the observation of relatively small perturbations of the dissolution front. Third, the experiment should be performed in a well controlled and reproducible manner. All of the above factors are effectively tackled by the use of microfluidic techniques.

In this letter, we present a simple microfluidic setup allowing for the direct observation of the onset of the reactive-infiltration instability and development of wormholes from an initially planar reaction front. We have designed an analog fracture which consists of a gypsum block inserted in between two polycarbonate plates and dissolved by water. This setup corresponds to a classical case of reactive infiltration, analogous to the processes taking place in reservoir stimulation or karst formation, although in our case only one side of the fracture is dissolving. The main advantage of our setup is the full control of the key parameters that influence the dissolution patterns along with a direct visual observation of the morphological evolution in real time.

2. Experimental Setup

In order to observe experimentally the onset of the reactive-infiltration instability, we have designed the experimental setup shown in Figure 1. It consists of two disks of 6.5 cm diameter and 1 cm thickness made of Makroclear®; polycarbonate. The bottom plate contains a rectangular indentation (3.3 cm × 3.8 cm × 0.5 mm) engraved using the MSG4025 CNC micro milling machine. This indentation serves as a cast for the plaster (Plaster of Paris, Blik Modelarski Alabastrowy) which is used as a soluble material in our system. The top plate contains a hierarchical system of inlet and outlet channels which are connected to large inlet/outlet reservoirs (4.5 cm × 5 mm × 2 mm). Such a design helps in keeping the uniform pressure along the width of the plaster. In order to keep the plates at a fixed distance, we insert between them a spacer made of the ultrathin PET-based double-coated tape of a thickness of either $h_0 = 100 \mu\text{m}$ (ORABOND 1394TM from ORAFOL GmbH), $h_0 = 70 \mu\text{m}$ (ORABOND 1398) or $h_0 = 210 \mu\text{m}$ (ORABOND 1397TM).

The cast was prepared with a 60% ratio (w/w) of water to plaster. This yields an average porosity of the block of $\phi = 50\%$ (measured porosity to water) and a permeability of 45 mD (measured by injection of isopropanol). A special care during the preparation has been put on the saturation of the medium with water in chemical equilibrium with the gypsum. Before the injection the chip is placed in vacuum within a beaker of saturated water in order to remove any air bubbles which might have remained in the pore space. Sealing is finally ensured with a silicone joint on the sides of the system.

After sealing, we connected the syringe pump (Harvard Apparatus PHD2000) to the chip to inject pure water. The applied flow rate ranged from 0.25 mL/h to 1 mL/h. We recorded the experiment with a UI 1550LE-C-HQ CCD camera (IOS, Germany), acquiring photographic images of the system every 100 s. In order to ensure homogeneous intensity of light over the system, we used a circular fluorescent illuminator.

Table 1. Values of the Parameters Relevant to the Experiments

Parameter	Experiment Symbol	Value							Precision
		1	2	3	4	5	6	7	
Initial aperture (μm)	h_0	100	70	210	100	70	70	100	$1\mu\text{m}$
Fracture width	L	3.3 cm							0.01 cm
Fracture length	–	3.8 cm							0.01 cm
Flow rate (mL/h)	q_0L	0.25	0.36	0.5	1	1	0.5	0.5	0.01 mL/h
Diffusion coefficient	D	$10^{-5} \text{ cm}^2/\text{s}$							$1 \cdot 10^{-7} \text{ cm}^2/\text{s}$
Reaction kinetic constant	k	$4.67 \cdot 10^{-4} \text{ cm/s}$							$0.07 \cdot 10^{-4} \text{ cm/s}$
									Can be larger depending on the impurity content
Ca^{2+} saturation concentration	c_{sat}	15 mol/m ³							0.1 mol/m ³
Gypsum molar volume	v	74.440 cm ³ /mol							$1.10^{-3} \text{ cm}^{-3}/\text{mol}$
Gypsum porosity	ϕ	50%							5%
Sherwood number	Sh	5							–

We ran seven different experiments on this setup whose characteristics are reported in Table 1. Additionally, experiments 1 and 2 (aperture 100 μm , flow rate 0.25 mL/h, aperture 70 μm , flow rate 0.36 mL/h) have been run twice while experiment 7 (aperture 100 μm and flow rate 0.5 mL/h) has been run 4 times in order to obtain an estimation of the repeatability.

3. Theoretical Model

The hydraulic resistance of the thin slot between the plastic roof and the plaster floor is significantly smaller than the resistance of the porous plaster itself. Hence, only a negligible fraction of the flow is directed into the plaster matrix. Since almost the entire flow is focused in the aperture space, the gypsum block is being dissolved from the top and the system can thus be looked upon as an analog of a fracture.

We chose Plaster of Paris as a soluble material because of the ease of handling and due to the relatively simple chemistry associated with its dissolution:



the kinetics of which is, to a good approximation, linear in the concentration of the calcium ions at the mineral surface, c_w [Colombani and Bert, 2007]

$$R(c_w) = k(c_{\text{sat}} - c_w) \quad (1)$$

with the intrinsic kinetic constant k and the saturation concentration c_{sat} . As we are considering the very early stages of the dissolution, the variation of the fracture aperture is relatively small. Consequently, we can model the system as quasi-two-dimensional [Oron and Berkowitz, 1998]. Moreover, considering also the low Reynolds number associated, we can approximate the flow in the slot space by the Reynolds equation for the local volume flux (per unit width), $\mathbf{q}(x, y) = \int_0^h \mathbf{v}(x, y, z) dz$:

$$\mathbf{q} = -\frac{h^3}{12\mu} \nabla p, \quad \nabla \cdot \mathbf{q} = 0, \quad (2)$$

where μ is the fluid viscosity. The transport of solute can be described in terms of flow-averaged concentration field, $\tilde{c}(x, y) = \frac{1}{q(x, y)} \int_0^h v(x, y, z) c(x, y, z) dz$ (the symbols used here are summarized in Table 1) [Hanna and Rajaram, 1998; Detwiler and Rajaram, 2007; Szymczak and Ladd, 2013]:

$$\nabla \cdot (\mathbf{q}\tilde{c} - D h \nabla \tilde{c}) = R \quad (3)$$

where D is the diffusion coefficient. To express the reactive current, R , in terms of average concentration, let us note that R needs to be balanced by the diffusive flux at the surface,

$$R = R_{\text{diff}} = -D(\nabla c)_w \cdot \mathbf{n} \quad (4)$$

where \mathbf{n} is the vector normal to the surface. The diffusive current can be expressed in terms of the geometry-dependent Sherwood number [Bird et al., 2001]

$$\text{Sh} = -\frac{2hR_{\text{diff}}}{D(c_w - \bar{c})} \quad (5)$$

The Sherwood number itself depends on kh/D , but the variation is relatively small [Gupta and Balakotaiah, 2001], bounded by two asymptotic limits; high reaction rates (transport limit) and low reaction rates (reaction limit). For our geometry (slot space with one dissolving wall) these limits correspond to $\text{Sh} = 4.861$ and $\text{Sh} = 5.385$, respectively [Ebadian and Dong, 1998]. In the theoretical calculations we approximate Sh by a constant value $\text{Sh} = 5$ (Table 1). Next, using (5) we express R_{diff} in terms of $(c_w - \bar{c})$ and equate it to R calculated based on (1). This leads to

$$c_w = \frac{1}{1 + \frac{2kh}{D\text{Sh}}} \left(\bar{c} + \frac{2kh}{D\text{Sh}} c_{\text{sat}} \right) \quad (6)$$

so that finally

$$R(\bar{c}) = k_{\text{eff}} (c_{\text{sat}} - \bar{c}) \quad (7)$$

where

$$k_{\text{eff}}(h) = \frac{k}{1 + 2kh/D\text{Sh}} \quad (8)$$

is an effective reaction rate which accounts for the diffusive slowdown of a reaction as the aperture increases. Finally, we have an equation for the aperture increase due to the dissolution of the porous matrix,

$$\frac{1 - \phi}{\nu} \partial_t h = k_{\text{eff}}(c_{\text{sat}} - \bar{c}), \quad (9)$$

where ν denotes the molar volume of gypsum and ϕ —its porosity. Note that, since $c_{\text{sat}}\nu \ll 1$, the characteristic timescale of the aperture evolution, $h_0/kc_{\text{sat}}\nu$ is much longer than the timescale of ion concentration relaxation (h_0/k). The slow dissolution of the surface allows the time dependence in (3) to be neglected.

Equations (2)–(9) clearly show the reason for the unstable nature of dissolution: any local increase of h will lead to the increased flow and faster dissolution, enhancing the phenomenon. Two different parameters control the behavior of the system: the Péclet number

$$\text{Pe} = \frac{q}{D}, \quad (10)$$

which characterizes the relative magnitude and diffusive transport, and the effective Damköhler number

$$\text{Da}_{\text{eff}} = \frac{k_{\text{eff}}(h_0)h_0}{q}, \quad (11)$$

relating the effective surface reaction rate, equation (8), to the rate of convective transport. Note that because in the experiment one can independently control both the flow rate (q) and the initial aperture (h_0), a full scan of the $\text{Pe}/\text{Da}_{\text{eff}}$ phase space is, in principle, possible. However, the domain where the initial instability can be observed is rather narrow, since it needs a sharp dissolution front and thus a relatively low flow rate (low Pe and high Da_{eff}).

The initial instability wavelength can be estimated theoretically by means of linear stability analysis of one-dimensional (planar) solutions of equations (2)–(9). The details of the derivation can be found in Szymczak and Ladd [2011, 2012]. The result of such an analysis is the dispersion curve, which gives the growth rate of the sinusoidal modes, which a front perturbation can be decomposed into. The position of the maximum of the dispersion curve corresponds to the fastest-growing mode, i.e., the one which is most likely to be observed in the experiment. Theoretical wavelengths corresponding to the experiments are presented in Table 2.

Table 2. The Characteristic Initial Instability Wavelength of the Dissolution Front^a

Experiment	Péclet	Effective Damköhler	Theoretical Wavelength		Measured Wavelength		Difference
			(mm)	Rescaled by h_0	(mm)		
1-a	2.058	0.191	3.50	35	3.47	2.5%	
1-b					3.17	9.4%	
2-a	2.963	0.0975	4.05	57.8	4.40	8.6%	
2-b					4.26	5.1%	
3	4.115	0.171	7.60	36.2	6.95	8.5%	
4	8.213	0.0478	11.0	110	11.9	10.9%	
5	8.213	0.0351	10.1	144	10.15	0.5%	
6	4.116	0.0794	5.31	75.8	5.12	3.6%	
7-a	4.116	0.0955	5.80	58	6.28	7.6%	
7-b					6.42	10.6%	
7-c					6.13	6%	
7-d					6.07	4.6%	

^aComparison between the experimental and the theoretical results.

4. Results and Discussion

Figure 2a presents several images taken at different points in time during the experiment 1. As observed, an initially planar front becomes unstable and breaks up in small protrusions. Initially, these perturbations are nearly sinusoidal, but soon the nonlinear effects in their dynamics become important—the protrusions transform into fingers, which then screen each other off, competing for the flow.

The analysis of the photographic images can be supplemented by the profilometry measurements of the chips using Bruker contour GT-K0 profilometer with 5X objective. This is an invasive method which requires to stop the experiment, open the Hele-Shaw cell, and dry the chip. Further evolution of the pattern after the profilometry measurement is then impossible. However, the comparison of the profilometry results with the photographic images of the system is important for the proper interpretation of the latter. The profilometry image (cf. Figure 2b) clearly shows the totally dissolved part of the chip on the right (marked in yellow) and the flat, undissolved portion of the chip on the left. The partially dissolved part in between the two captures the beginning of the instability with gouges appearing on the initially flat front. The corresponding photo, taken just before the dismantling of the setup for profilometry measurement is shown in Figure 2c. Here the totally dissolved part is black, whereas partially dissolved regions show up as light grey.

Since the results obtained with the linear stability analysis correspond to the very initial stage of the spontaneous front breakup, it is necessary to measure the instability wavelength as early as possible. To this end, we extracted the shape of the dissolution front from the photographic images and applied a Fast Fourier Transform (FFT) algorithm to this data in order to decompose the signal into the sinusoidal modes. The position of the maximum of the spectrum corresponds to the fastest-growing mode, which the theory is able to predict. Because of the finite width of the system, the spectrum is defined at the discrete wave numbers only. In order to interpolate the spectrum between the discrete points, we used the zero-padding technique. Additionally, in order to limit the boundary effects and reduce frequency leakage, we applied a classical Blackman window which presents a good compromise between the width of the central peak and an attenuation of the side lobes [Brigham, 1988]. An example of the Fourier spectrum obtained with this technique is presented in Figure 3 (top). The highest peak corresponds to the dominant wavelength of the instability. The other two peaks are, respectively, twice the dominant wavelength and a wavelength associated with the size of the system. The latter appears due to the boundary effects. The appearance of the former, on the other hand, has its origin in a screening process between the fingers, as a result of which approximately half of them become arrested in their growth, whereas the other half continues to grow [Huang *et al.*, 1997; Budek *et al.*, 2015].

Table 2 summarizes the results for the measurement of the characteristic instability wavelength. The comparison between the experimental measurements and the theoretical predictions presents a very good agreement, well within the error bars. Still, there are some uncertainties regarding the data shown in Table 1,

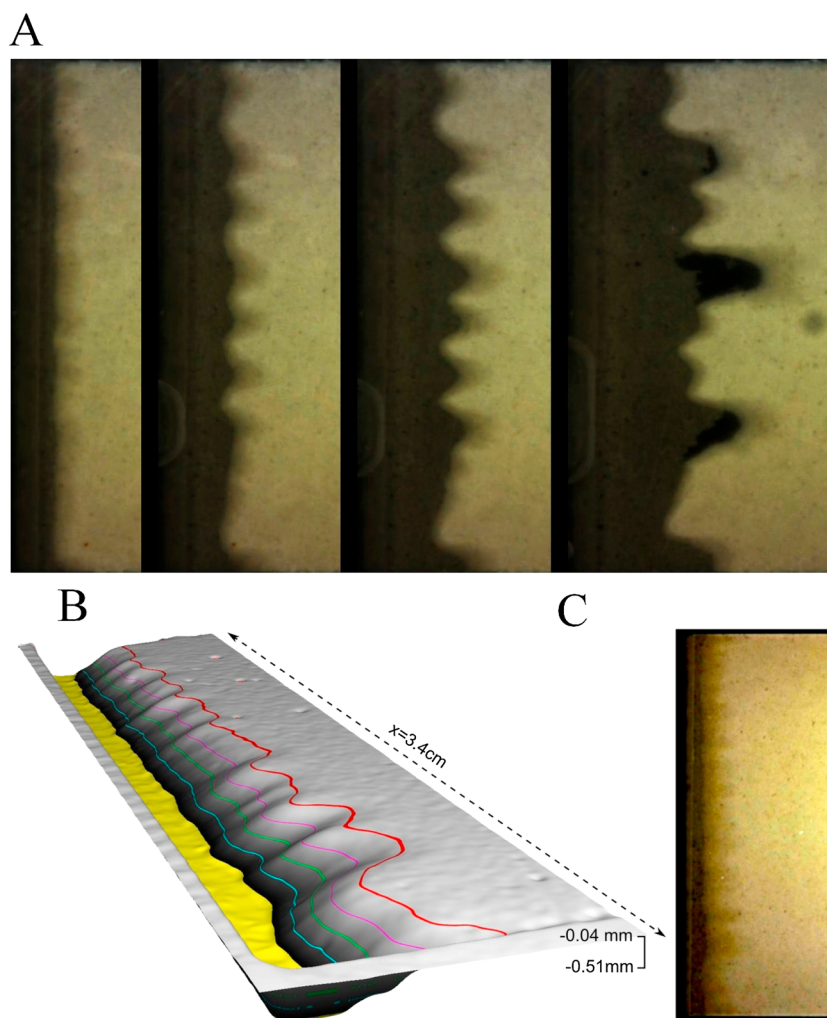


Figure 2. (a) Advancement of the dissolution front and the onset of the instability for experiment 1-a. The successive times correspond to 4.3, 6.2, 8.3, and 10.8 days. (b) Image from the profilometry measurement performed on experiment 7-a plaster chip after 2 days of injection. (c) The photographic image corresponding to Figure 2b.

which impose error bars on our theoretical estimate. First of all, there is an uncertainty associated with the estimate of the gypsum dissolution rate, which can vary depending on, for example, impurity content [Jamtveit and Meakin, 1999]. We have taken the value of $k = 4.67 \cdot 10^{-4}$ cm/s for the gypsum dissolution rate constant [Colombani, 2008] as the one corresponding to an average over all crystallographic orientations of gypsum, which should most faithfully represent the properties of our sample. Second, there are uncertainties regarding the initial aperture, the width of the system, and the flow rate, leading to the uncertainty on the Péclet and Damköhler numbers of 5% and 10%, respectively. A strong indicator of the correctness of the method is the repeatability—different runs of the experiments provide similar results.

Figure 3 (bottom) shows the theoretically calculated dominant instability wavelength (normalized by the initial aperture) in the Pe/Da_{eff} domain, with crosses marking the positions corresponding to the experimental conditions. It is worth noting that in the region of this domain which can be effectively probed by our setup (i.e., $Pe > 1$) the normalized wavelength λ/h_0 is controlled almost completely by Da_{eff} —the larger the effective Damköhler number, the smaller the dominant wavelength is. The influence of the Péclet number gets larger toward smaller Pe , but this region of the domain is unfortunately unreachable in the experiments, as it would require very long experimental runs and very thin (less than $50 \mu\text{m}$) double-coated tape. On the other hand, at large Péclet numbers, the penetration length of the reactant becomes comparable with the size of the system. As a result, the sample then dissolves uniformly [Hoefner and Fogler, 1988; Golfier et al., 2002] and the

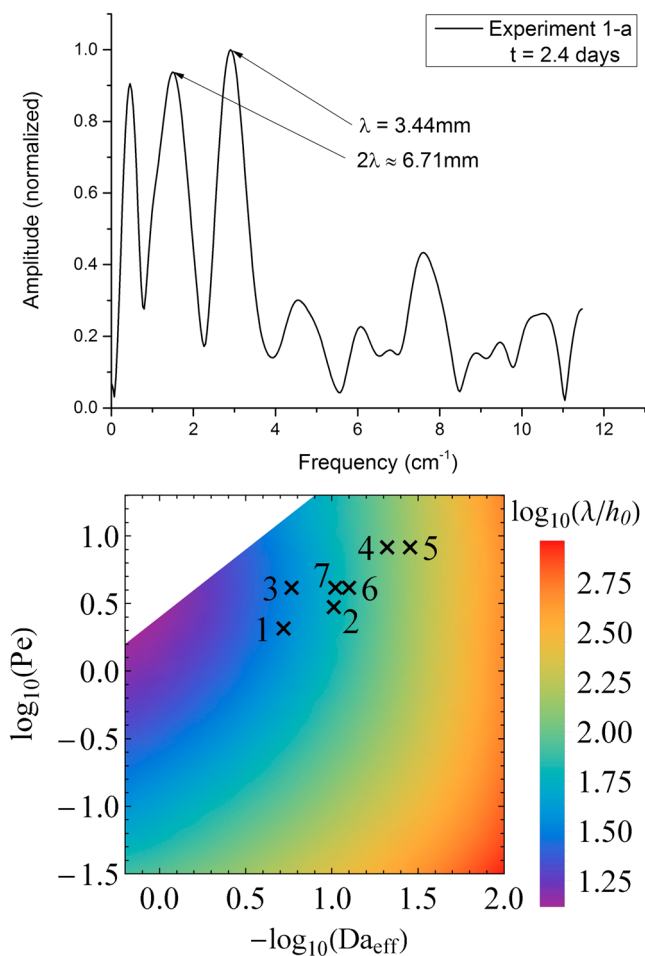


Figure 3. (top) Spectral analysis of the dissolution front for experiment 1-a. The position of the highest peak agrees well with the theoretical prediction. Other peaks correspond to the nonlinear couplings between the modes, boundary effects, roughness of the system, artifacts of the windowing, or are harmonics of the main wavelength. (bottom) The instability wavelength (normalized by the aperture), λ/h_0 , as a function of the Péclet (Pe) and effective Damköhler (Da_{eff}) number. The positions corresponding to the experimental conditions are marked by crosses. The white region in the top left part of the plot is unreachable (as it would require a negative kinetic constant k).

development of the instability cannot be observed. The above factors limit the region of the domain where the wavelength can be effectively measured.

5. Conclusions

The theory of instabilities and fingering induced by reactive flow in porous media has been intensively developed and the associated physics is well understood. However, it was difficult up to now to provide experimental evidence of the onset of the instability because of the inherent issues associated with experiments with natural rocks.

The experimental setup described here allows for a direct observation of the first stages of the instability. We find a very good agreement between the experimental results and the theoretical wavelength of the initial instability calculated performing the linear stability analysis. Interestingly, this experiment can also be used to measure the intrinsic reaction rate of minerals. Indeed, by replacing gypsum with any compacted mineral powder and running a dissolution experiment, one can extract the initial instability wavelength and actually measure the associated effective Damköhler number. As the reaction rate is typically difficult to extract [Colombani, 2008; Raines and Dewers, 1997] because of the couplings of chemical reaction and transport of products, our technique could provide an interesting alternative method for the determination of this quantity.

Finally, let us note that one of the reasons why the theory based on the quasi-2-D approximation (equations (2)–(8)) works so well is that the instability development and wavelength selection takes place early on, when the aperture is nearly constant, $h \approx h_0$. In the later stages of the dissolution, however, as the aperture becomes nonuniform, 3-D effects begin to play a role. In particular, we have found that the quasi-2-D approximation tends to underestimate the slope of the dissolution profile, dh/dx , at its upstream part by about 10–20%.

Acknowledgments

F.O., A.B., P.K., and P.S. acknowledge the support of the National Science Centre (Poland) under research grant 2012/07/E/ST3/01734. O.C. and P.G. acknowledge the support within the European Research Council Starting grant 279647. P.G. acknowledges also the support within the Mistrz programme from the Foundation for Polish Science. The authors wish to thank Jean Colombani from the University of Lyon for very useful discussions on the reaction rate of gypsum and ROLLFIX®; for providing us the tape used in the experiments. The authors also benefited from discussions with Amélie Neuville, Dag Dysthe, and Tony Ladd. All data and related metadata underlying the findings reported can be requested by e-mail from piotr.szymczak@fuw.edu.pl.

References

- Aharonov, E., J. Whitehead, P. Kelemen, and M. Spiegelman (1995), Channeling instability of upwelling melt in the mantle, *J. Geophys. Res.*, *100*, 433–455.
- Bird, R. B., W. E. Stewart, and E. N. Lightfoot (2001), *Transport Phenomena*, John Wiley, Dept. of Chem. Eng., Madison, Wis.
- Brigham, O. E. (1988), *The Fast Fourier Transform and its Applications*, Prentice Hall Signal Process. Ser., Upper Saddle River, N. J.
- Budek, A., P. Garstecki, A. Samborski, and P. Szymczak (2015), Thin-finger growth and droplet pinch-off in miscible and immiscible displacements in a periodic network of microfluidic channels, *Phys. Fluids*, *27*(11), 112109.
- Cabeza, Y., J. J. Hidalgo, and J. Carrera (2015), Controlling factors of wormhole growth in Karst aquifers, in *Hydrogeological and Environmental Investigations in Karst Systems*, pp. 379–385, Springer, Berlin.
- Carroll, S., Y. Hao, M. Smith, and Y. Sholokhova (2013), Development of scaling parameters to describe CO₂-rock interactions within Weyburn-Midale carbonate flow units, *Int. J. Green Gas Con.*, *16*, S185–S193.
- Chadam, D., D. Hoff, E. Merino, P. Ortoleva, and A. Sen (1986), Reactive infiltration instabilities, *J. Appl. Math.*, *36*, 207–221.
- Cioabanu, C. L., and N. J. Cook (2004), Skarn textures and a case study: The Ocna de Fier-Dognecea orefield, Banat, Romania, *Ore Geol. Rev.*, *24*, 315–370.
- Colombani, J. (2008), Measurement of the pure dissolution rate constant of a mineral in water, *Geochim. Cosmochim. Acta*, *72*, 5634–5640.
- Colombani, J., and J. Bert (2007), Holographic interferometry study of the dissolution and diffusion of gypsum in water, *Geochim. Cosmochim. Acta*, *71*, 1913–1920.
- Daccord, G. (1987), Chemical dissolution of a porous medium by a reactive fluid, *Phys. Rev. Lett.*, *58*(5), 479–482.
- Daccord, G., and R. Lenormand (1987), Fractal patterns from chemical dissolution, *Nature*, *325*, 41–43.
- Dahlkamp, F. J. (2009), *Uranium Deposits of the World*, Springer, Berlin.
- Daines, M. J., and D. L. Kohlstedt (1994), The transition from porous to channelized flow due to melt/rock reaction during melt migration, *Geophys. Res. Lett.*, *21*, 145–148.
- Deng, H., B. R. Ellis, C. A. Peters, J. P. Fitts, D. Crandall, and G. S. Bromhal (2013), Modifications of carbonate fracture hydrodynamic properties by CO₂-acidified brine flow, *Energy Fuels*, *27*(8), 4221–4231.
- Detwiler, R. L., and H. Rajaram (2007), Predicting dissolution patterns in variable aperture fractures: Evaluation of an enhanced depth-averaged computational model, *Water Resour. Res.*, *43*, W04403, doi:10.1029/2006WR005147.
- Detwiler, R. L., R. J. Glass, and W. L. Bourcier (2003), Experimental observations of fracture dissolution: The role of Péclet number in evolving aperture variability, *Geophys. Res. Lett.*, *30*, 1648, doi:10.1029/2003GL017396.
- Ebadian, M. A., and Z. F. Dong (1998), Forced convection, internal flow in ducts, *Handbook of Heat Transfer*, edited by W. M. Rohsenow, J. P. Hartnett, and Y. I. Cho, chap. 5, McGraw-Hill, New York.
- Elkhoury, J., R. Detwiler, and P. Ameli (2015), Can a fractured caprock self-heal?, *Earth Planet. Sci. Lett.*, *417*, 99–106.
- Elkhoury, J. E., P. Ameli, and R. L. Detwiler (2013), Dissolution and deformation in fractured carbonates caused by flow of CO₂-rich brine under reservoir conditions, *Int. J. Greenh. Gas Con.*, *16*, S203–S215.
- Ellis, B. R., C. A. Peters, J. P. Fitts, G. S. Bromhal, D. McIntyre, R. Warzinski, and E. Rosenbaum (2011), Deterioration of a fractured carbonate caprock exposed to CO₂-acidified brine flow, *Greenhouse Gases*, *1*(3), 248–260.
- Fu, X., L. Cueto-Felgueroso, D. Bolster, and R. Juanes (2015), Rock dissolution patterns and geochemical shutdown of brine-carbonate reactions during convective mixing in porous media, *J. Fluid Mech.*, *764*, 296–315.
- García Ríos, M. (2015), Dissolved CO₂ effect on the reactivity of the Hontominí reservoir rocks (limestone and sandstone), PhD thesis, Tech. Univ. of Catalonia, Barcelona, Spain.
- Golfier, F., C. Zarcone, B. Bazin, R. Lenormand, D. Lasseux, and M. Quintard (2002), On the ability of a Darcy-scale model to capture wormhole formation during the dissolution of a porous medium, *J. Fluid Mech.*, *457*, 213–254.
- Groves, C. G., and A. D. Howard (1994), Early development of karst systems. I. Preferential flow path enlargement under laminar flow, *Water Resour. Res.*, *30*, 2837–2846.
- Gupta, N., and V. Balakotaiah (2001), Heat and mass transfer coefficients in catalytic monoliths, *Chem. Eng. Sci.*, *56*(16), 4771–4786.
- Hanna, R. B., and H. Rajaram (1998), Influence of aperture variability on dissolution growth of fissures in karst formations, *Water Resour. Res.*, *34*, 2843–2853.
- Hao, Y., M. Smith, Y. Sholokhova, and S. Carroll (2013), CO₂-induced dissolution of low permeability carbonates. Part II: Numerical modeling of experiments, *Adv. Water Res.*, *62*, 388–408.
- Hidalgo, J. J., M. Dentz, Y. Cabeza, and J. Carrera (2015), Dissolution patterns and mixing dynamics in unstable reactive flow, *Geophys. Res. Lett.*, *42*, 6357–6364, doi:10.1002/2015GL065036.
- Hinch, E. J., and B. S. Bhatt (1990), Stability of an acid front moving through porous rock, *J. Fluid Mech.*, *212*, 279–288.
- Hoefner, M. L., and H. S. Fogler (1988), Pore evolution and channel formation during flow and reaction in porous media, *Am. Inst. Chem. Eng. J.*, *34*, 45–54.
- Huang, Y., G. Ouillon, H. Saleur, and D. Sornette (1997), Spontaneous generation of discrete scale invariance, *Phys. Rev. E*, *55*, 6433–6447.
- Jamtveit, B., and P. Meakin (1999), *Growth, Dissolution and Pattern Formation in Geosystems*, Springer, Netherlands.
- Kalia, N., and V. Balakotaiah (2009), Effect of medium heterogeneities on reactive dissolution of carbonates, *Chem. Eng. Sci.*, *64*, 376–390.
- Kelemen, P., J. Whitehead, E. Aharonov, and K. Jordahl (1995), Experiments on flow focusing in soluble porous media, with applications to melt extraction from the mantle, *J. Geophys. Res.*, *100*, 475–496.
- Luquot, L., and P. Gouze (2009), Experimental determination of porosity and permeability changes induced by injection of CO₂ into carbonate rocks, *Chem. Geol.*, *265*(1–2), 148–159.
- Luquot, L., O. Rodriguez, and P. Gouze (2014), Experimental characterization of porosity structure and transport property changes in limestone undergoing different dissolution regimes, *Transport Porous Med.*, *101*(3), 507–532.

- Menke, H. P., B. Bijeljic, M. G. Andrew, and M. J. Blunt (2015), Dynamic three-dimensional pore-scale imaging of reaction in a carbonate at reservoir conditions, *Environ. Sci. Tech.*, *49*(7), 4407–4414.
- Merino, E. (2011), Self-accelerating dolomite-for-calcite replacement: Self-organized dynamics of burial dolomitization and associated mineralization, *Am. J. Sci.*, *311*, 572–607.
- Noiriel, C., P. Gouze, and B. Made (2013), 3D analysis of geometry and flow changes in a limestone fracture during dissolution, *J. Hydrol.*, *486*, 211–223.
- Oron, A. P., and B. Berkowitz (1998), Flow in rock fractures: The local cubic law assumption reexamined, *Water Resour. Res.*, *34*, 2811–2825.
- Ortoleva, P., J. Chadam, E. Merino, and A. Sen (1987), Geochemical self-organization II: The reactive-infiltration instability, *Am. J. Sci.*, *287*, 1008–1040.
- Ortoleva, P. J. (1994), *Geochemical Self-Organization*, Oxford Univ. Press, New York.
- Ott, H., and S. Oedai (2015), Wormhole formation and compact dissolution in single-and two-phase CO₂-brine injections, *Geophys. Res. Lett.*, *42*, 2270–2276.
- Pec, M., B. K. Holtzman, M. Zimmerman, and D. L. Kohlstedt (2015), Reaction infiltration instabilities in experiments on partially molten mantle rocks, *Geology*, *43*, 575–578.
- Polak, A., D. Elsworth, J. Liu, and A. S. Grader (2004), Spontaneous switching of permeability changes in a limestone fracture with net dissolution, *Water Resour. Res.*, *40*, W03502, doi:10.1029/2003WR002717.
- Raines, M. A., and T. A. Dewers (1997), Mixed transport/reaction control of gypsum dissolution kinetics in aqueous solutions and initiation of gypsum karst, *Chem. Geol.*, *140*, 29–48.
- Rowan, G. (1959), Theory of acid treatment of limestone formations, *J. Inst. Pet.*, *45*(431), 321–334.
- Sherwood, J. D. (1987), Stability of a plane reaction front in a porous medium, *Chem. Eng. Sci.*, *42*, 1823–1829.
- Smith, M., Y. Sholokhova, Y. Hao, and S. Carroll (2013), CO₂-induced dissolution of low permeability carbonates. Part I: Characterization and experiments, *Adv. Water Resour.*, *62*, 370–387.
- Spiegelman, M., P. Kelemen, and E. Aharonov (2001), Causes and consequences of flow organization during melt transport: The reaction infiltration instability in compactable media, *J. Geophys. Res.*, *106*, 2061–2077.
- Steeffel, C. I., and A. C. Lasaga (1990), Evolution of dissolution patterns, in *Chemical Modeling of Aqueous Systems II*, edited by D. C. Melchior and R. L. Bassett, pp. 212–225, Am. Chem. Soc, Washington, D. C.
- Szymczak, P., and A. Ladd (2011), The initial stages of cave formation: Beyond the one-dimensional paradigm, *Earth Planet. Sci. Lett.*, *301*, 424–432.
- Szymczak, P., and A. J. C. Ladd (2012), Reactive infiltration instabilities in rocks. Fracture dissolution, *J. Fluid Mech.*, *702*, 239–264.
- Szymczak, P., and A. J. C. Ladd (2013), Interacting length scales in the reactive-infiltration instability, *Geophys. Res. Lett.*, *40*, 3036–3041.
- Szymczak, P., and A. J. C. Ladd (2014), Reactive infiltration instabilities in rocks. Part 2. Dissolution of a porous matrix, *J. Fluid Mech.*, *738*, 591–630.
- Upadhyay, V. K., P. Szymczak, and A. J. Ladd (2015), Initial conditions or emergence: What determines dissolution patterns in rough fractures?, *J. Geophys. Res. Solid Earth*, *120*, 6102–6121, doi:10.1002/2015JB012233.